Fachtagung "Lasermethoden in der Strömungsmesstechnik"
9. – 11. September 2014, Karlsruhe

Analysis of flow phenomena within the side channel of a regenerative pump by means of HS- SPIV and POD

Untersuchung von Strömungsphänomenen im Seitenkanal einer Seitenkanalmaschine mit HS-SPIV und POD

Philipp Mattern [1], Maximilian Elfner [2], Jochen Kriegseis [3], Martin Gabi [4]
1,4: Fachgebiet Strömungsmaschinen(FSM), Karlsruher Institut für Technologie (KIT)
2: Institut für Thermische Strömungsmaschinen, Karlsruher Institut für Technologie (KIT)
3: Institut für Strömungsmechanik, Karlsruher Institut für Technologie (KIT)

High Speed Stereo PIV, POD, Seitenkanalpumpe, Strömungsmaschinen, Helix
High Speed Stereo PIV, POD, side channel pump, regenerative pump, fluid machinery, helix

Abstract

To understand the complex flow phenomena within a regenerative pump, the side channel of a generic model with a diameter of 200 mm is examined by means of Highspeed- Stereo Particle Image Velocimetry (HS SPIV). It is shown, that by analyzing the data using a proper orthogonal decomposition (POD) a significantly deeper understanding of the complex flow within the machine can be achieved compared to the classic approach of time and spatial as well as phase averaging. Particularly, the strong influence of the all-concealing average flow can be minimized.

Introduction

Regenerative pumps are characterized by very high specific pressure heads and low specific flow rates. As such, they cover a special field of application, which to date has been rarely documented in public literature. They are self-priming and their working principle is "quasi multistage". Since their efficiency is relatively low compared to the more common axial or radial types, advanced optimization strategies are of utmost importance for the development of such pumps. The purpose of the present study therefore addresses the identification of the coherent flow patterns in game. Particularly, characterization of the helicoidal flow structure interacting between the impeller and the side channel provides a deeper inside into the involved cause-effect-relations. In order to obtain the desired flow information, a generic model (Figure 1) with full optical accessibility has been designed and integrated in a classic pump test rig to enable a detailed examination by means of HS SPIV.

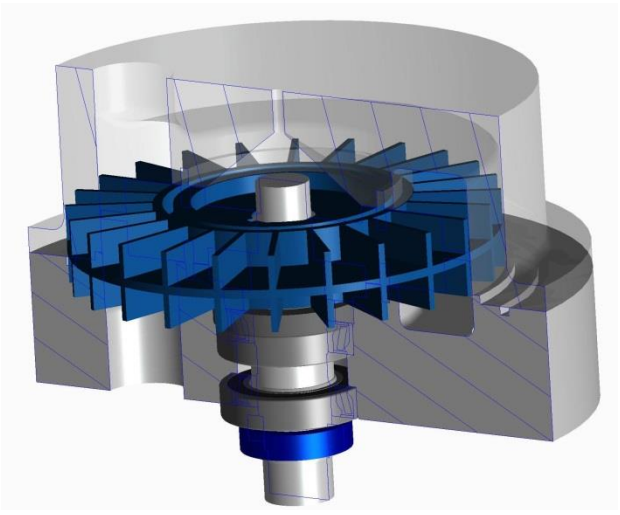

Figure 1: CAD Model of the regenerative pump

Experimental setup

Figure 1 shows the generic model. The impeller with its 24 blades is covered by an acrylic casing with the side channel integrated. Although a double flow machine was realized due to symmetrical reasons, only the upper flow was examined. The machine is running at a speed of 500 rpm near its best point of operation. The classic layout of the test rig allows full control over the flow regime and therefore the operation point of the machine. To illustrate the flow through the machine, Figure 2 is introduced. The fluid enters the machine at the upper right corner and is circularly transported along θ through the side channel to the outlet (This defines the main flow). z defines the axial coordinate, while θ and r are defined in cylindrical coordinates. Note that in- and outlet are separated by a stripper (hatched Area), which is used as the origin of the circumferential coordinate θ. The light sheet of the Laser enters the acrylic casing from the left side and illuminates the area marked in red. The transport mechanism behind that is described by an axial interaction between the flow in the side channel and the blades of the impeller (secondary flow). This secondary flow is shown in red in Figure 3. The Stereo PIV System is set up in a standard Forward/Backward scattered Setup, with an angle of 65° between both cameras and a distance of 340 mm between the cameras and the light sheet. The flow is captured at 2000 fps with a resolution of 1 Megapixel. More details of the experimental setup can be found in [1].

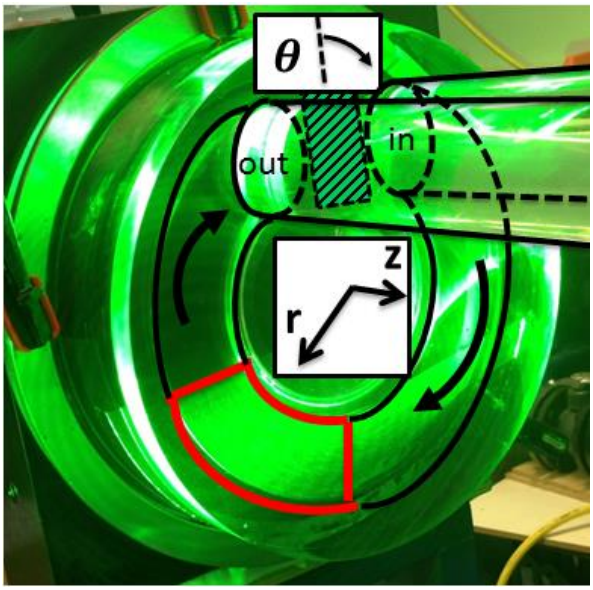

Figure 2: Acrylic Side Channel with marked PIV Measurement Position (red area)

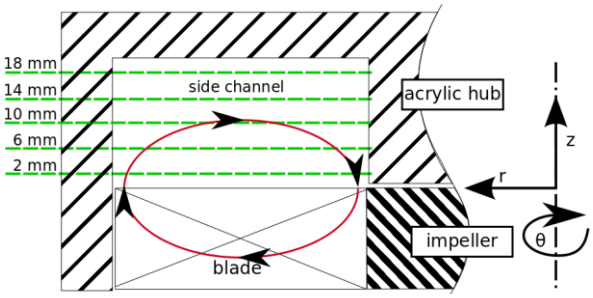

Figure 3: Measurement planes (dotted green) with superimposed secondary flow (red)

Post-processing

For PIV Analysis PIVTEC's PIVview (V3.5.9.1) is used. Common methods of dewarping and disparity correction are applied. The cross correlation has an interrogation area of 12x12 pixels and an overlap of 50%. A strict dynamic mean filter of 2*mean velocity +- 1*standard deviation leads to a small amount of around 2% invalid vectors. Half of them are interpolated; the other ones are taken from other correlation peaks. Separation Time (Pulse Distance) between the two pulses is 75 µs. During 1.4 seconds of measurement, 2770 velocity maps for an area of 110x50 mm each containing more than 8000 three component vectors are captured. Customized post-processing Algorithms have been applied for any further analysis of the velocity data.

Basics: Proper Orthogonal Decomposition (POD)

The POD method decomposes a temporally and spatially resolved turbulent flow field $\boldsymbol{u}(\boldsymbol{x},t) = \mathbf{U}(\mathbf{x},\mathrm{t}) - \overline{\boldsymbol{U}(\boldsymbol{x})}$ into its spatial POD modes $\phi_j(\boldsymbol{x})$ (Eigenvector fields) and its corresponding energy contents λ_j (Eigenvalues). The linearly independent POD modes form a new base for the flow field, identifying coherent (reoccurring) flow patterns by a high modal energy and thus separating them from incoherent, random fluctuations with low modal energy. Subtracted from the mean flow, velocity fluctuations (u^n) at every time step n are collected and are used to build the covariance matrix **C:**

$$\boldsymbol{V} = [\boldsymbol{u}^1 \dots \boldsymbol{u}^n \dots \boldsymbol{u}^N], \quad \boldsymbol{C} = \boldsymbol{V}^T\boldsymbol{V} .$$

Solving the Eigenvalue problem of **C** leads to $j = 1..N$ Eigenvalue/Eigenvector combinations. The Eigenvalues λ_j are normalized and considered as the modal energies P_j. The intermediate Eigenvectors $\boldsymbol{A}_j$ are then projected on the flow field and normalized to obtain the spatial Eigenvector field $\phi_j(\boldsymbol{x})$:

$$\phi_j(\boldsymbol{x}) = \frac{A_j^n \boldsymbol{u}^n}{\left\| A_j^n \boldsymbol{u}^n \right\|}$$

Finally, the Eigenvalues and corresponding Eigenvector fields are sorted decreasing, ordering in coherent structures up front. Back transformation ('reconstruction') to the temporal domain is then done by series expansion:

$$\boldsymbol{u}^n(\boldsymbol{x}) = \boldsymbol{a}_j^n \phi_j(\boldsymbol{x})$$

The weighting coefficients a_j can be determined by inverting the equation above using the full number of modes available. During practical reconstruction, truncation is possible and done for filtering. Truncation criteria need to be determined manually and flow field specific. For more comprehensive description of the POD method, the reader is referred to [2, 3].

In Summary, the POD Analysis decomposes a given flow field into energy-weighted flow patterns whose recombination (back transformation) results in the original flow field.

Averaged Results

In a first approach the resulting vector maps are time averaged. Figure 4 shows this exemplarily for the 2 mm measurement plane. θ is with respect to the stripper (see Figure 2). It is clearly visible, that the average in plane velocity of 3 m/s is significantly higher than the axial component shown as the contour plot. For a better understanding of the secondary flow the unrolled side channel is introduced in Figure 5. The flow direction changes over the radius, which already provides

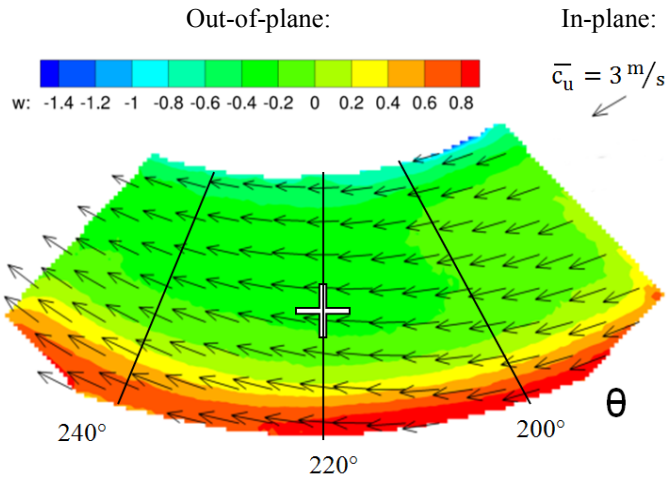

Figure 4: PIV results of the normalized circumferential velocities at 500 rpm at the 2 mm position

some confidence on the existence of the heliciodal structure of the flow. By using the angle of rotation as additional information, it is possible to do phase averaging. As shown in Figure 6, it now becomes visible that the flow within the side channel is strongly influenced by the blades, giving the flow field a pattern-like structure moving along with θ. Furthermore, a salient wavelike structure of the main flow is now uncovered at the outer wall. Spurious vectors due to blade reflections have been eliminated. The high positive axial velocities on the pressure side of the blade can be explained, as the fluid is blocked by the casing. Consequently, it cannot be transported furthermore along the radius and therefore has to evade to the only direction left (upwards into the side channel). The necessary negative backflow into the blade channel is now more obvious. Although around 150 velocity maps were averaged for each figure, there remain considerable amounts of noise, additionally superimposed by recombination errors in the upper left corner.

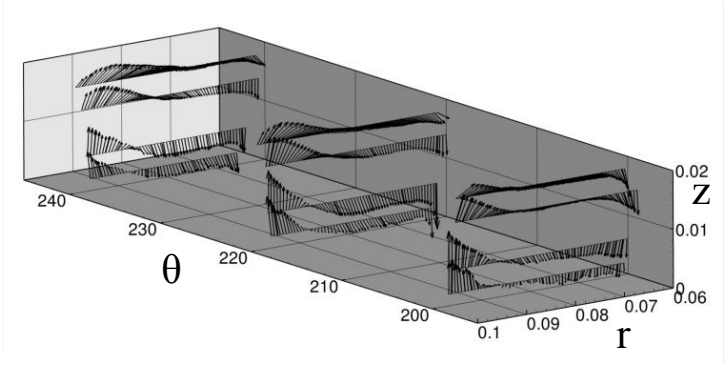

Figure 5: Normalized secondary flow within the side channel at 500 rpm

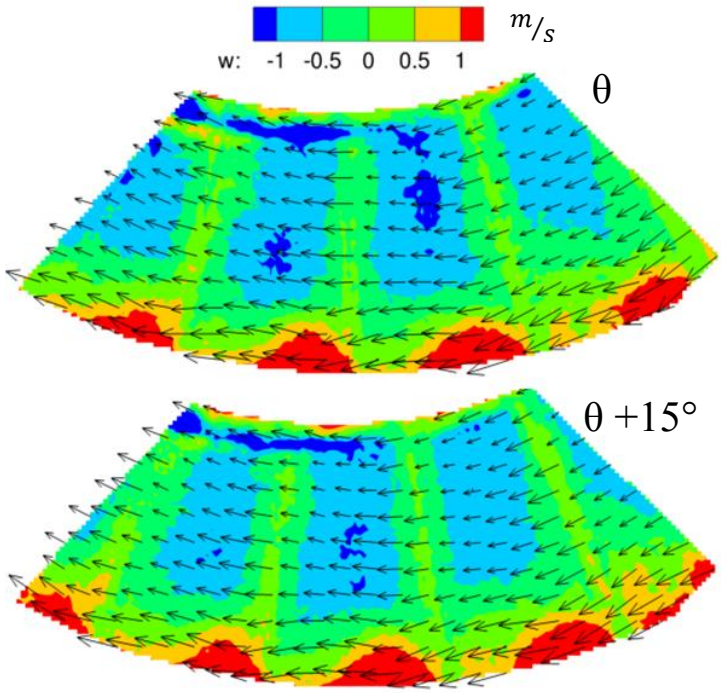

Figure 6: Phase Averaged Mean Velocities for different angles

Unsteady Phenomena

To understand the highly unsteady behavior of the flow, the fluctuation of the circumferential velocity at a point in the middle of the measurement plane (white cross in Figure 4) is shown in Figure 7. An underlying periodic oscillation is recognizable. Using a Fast Fourier Transformation, a frequency of 200 Hz can clearly be identified. This is explainable by the blade passing frequency of:

$$\frac{number\ of\ blades * rpm}{60} = \frac{24 * 500}{60} = 200\ Hz$$

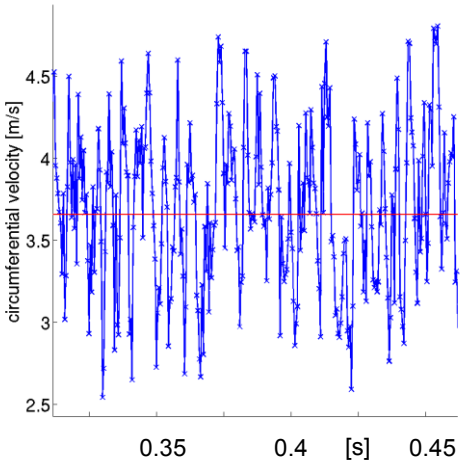

Figure 7: Circumferential velocity fluctuation over time

While passing through the stripper, the strong pressure gradient against the inlet cannot be reduced completely, leading to a pressure surge at the end of the stripper. This surge superimposes the flow through the side channel and is detectable. This was already recognized by Surek [4], who identified the blade passing frequency as the dominating frequency in pressure fluctuations at the outer wall of a common side channel machine. In addition he identified higher frequencies, which were hypothesized to the forced turbulent vortex swirl flow at the trailing edge of the blades. The existence of such vortical structures can hardly be identified when looking at the velocity-pattern in the phase averaged figures (Figure 6). To overcome these shortcomings, the more rigorous approach of the POD Analysis is applied to uncover the contained flow pattern.

POD Results

The Analysis of the POD results can be split into 3 steps:
First, the modal structures and their energy contributions to the flow are investigated. The 2700 discrete velocity fields per measurement result in the same amount of POD modes.
Subsequently, the weighting coefficients a_j are calculated and their time dependent behavior is investigated.
Finally, with the information from the energy spectrum and the weighting coefficient's temporal distribution, a fitting truncation criterion can be established, which allows an energy filtered reconstruction of the original turbulent flow field.

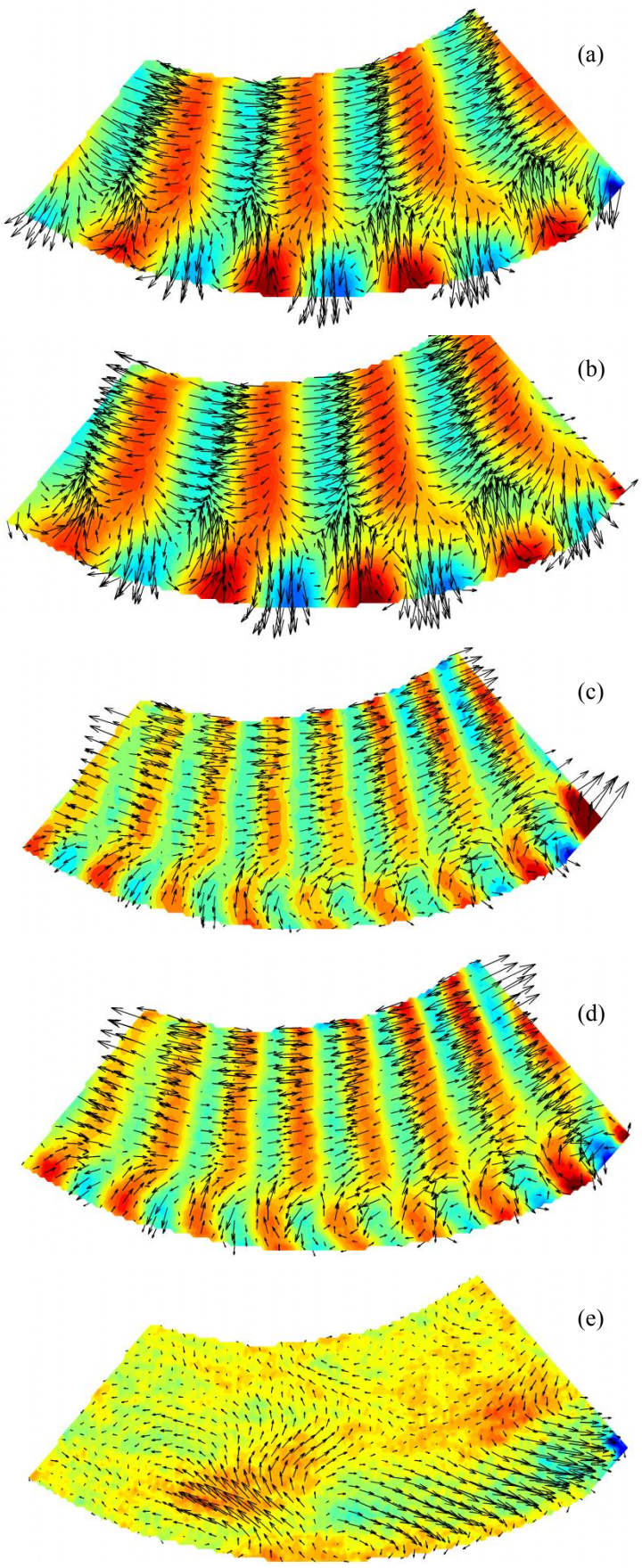

Figure 8: POD Mode 1(a), Mode 2 (b), Mode 3 (c), Mode 4 (d), Mode 6 (e)

This evaluation will be exemplarily shown for the measurement plane at 2 mm distance to the impeller (compare Figure 3):

Figure 8 shows the first four modes and mode number six. Modal patterns are shown as vectors for the in-plane and as contour plot for the out-of-plane component.

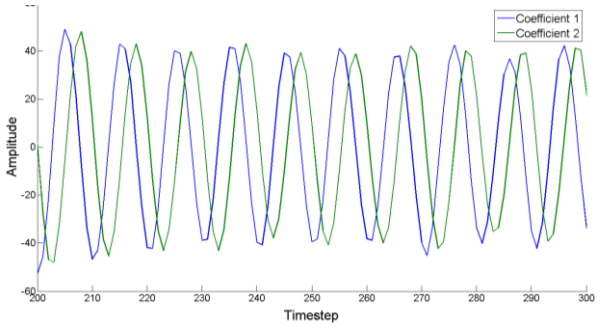

Figure 9: Weighting coefficients Mode 1 and Mode 2

The first two modes, as well as Mode 3 and 4, reveal very similar flow patterns. Both show blade related flow structures in plane, as well as out-of-plane, with flow patterns analogous to Figure 6. However, a system of interacting vortices can now be observed at the outer diameter of the side channel. This system shows pairs of counter-rotating vortices, which are assumed to be the effect of the trailing edges of the blades interacting with the outer wall of the side channel (an exact interpretation is subject to further investigations). A distinct difference between Mode 1 and 2 is the fact, that the structures are shifted by a certain angle in flow direction. This 90°-phase shift becomes more obvious from the reconstructed coefficient of the respective modes, as shown in Figure 9. The coefficient oscillation again reveals the blade passing frequency of 200 Hz. Note that the 90°-phase shift at identical frequency is verified by the circular shape of the corresponding Lissajous figure (Figure 10b).

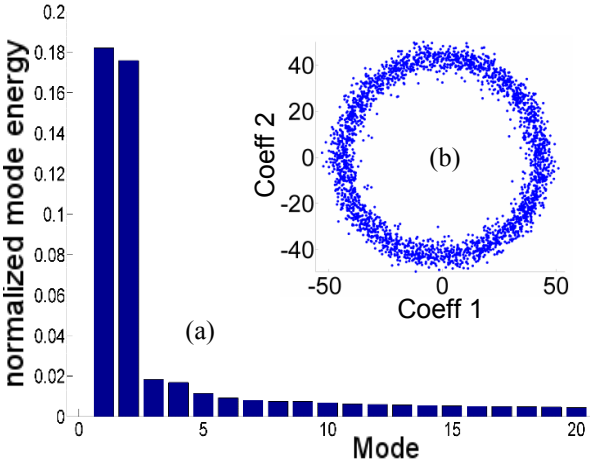

Figure 10: Energy spectrum (a) and Lissajous Figure of Mode 1&2 (b)

The energy spectrum for the first 20 Modes is introduced with Figure 10a. Combined, Modes 1 and 2 contain approximately 35% of the flows turbulent energy. The directly following modes 3 and 4 already show a huge decrease in energy. Nevertheless they show blade related patterns at a doubled frequency and are not to be neglected.

To further understand the physical meaning of the shown modal structures, the retransformation to the temporal domain is further analyzed. It explains the similarity between Modes 1 and 2. By alternating between the two shifted structures with blade passing frequency, the visible blade structures and vortex systems in either mode are moved through the temporal domain, following the blades. It indicates the driving force behind mass transportation through the system.

Mode 6 (see Figure 8e) already contains only about 1% of the total energy. This Mode is added exemplarily as the strongest of all low-energy bearing Modes, showing no structures obviously related to any parameter of the machine. From there on, the modal energies asymptotically approach a constant value, making them statistically similar. This is a strong indicator for random noise.

In conclusion, a combination of Mode 1 and Mode 2 is already a good resemblance of the instantaneous turbulent flow field, containing about 35% of the flows energy for the near-blade planes.

However, to reconstruct a meaningful flow field, additional (lower-energetic) modes have to be superimposed. Following the above analysis, a low number of modes is sufficiently enough for the reconstruction of the flow patterns.

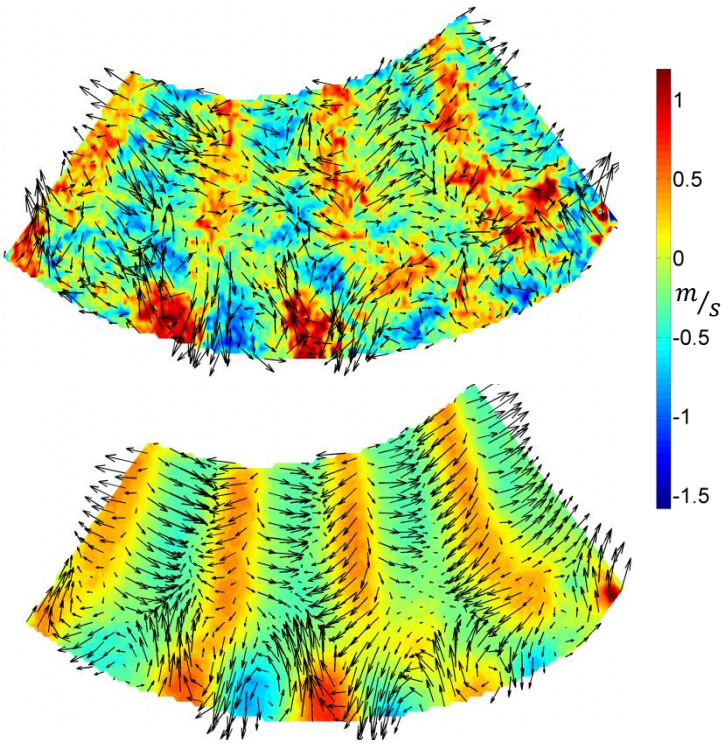

Figure 11: Comparison original (top) vs. reconstructed (bottom) flow field

Figure 11 shows the comparison between the original and the reconstructed flow field (approximately 30 modes, or 60% of turbulent flow energy) for a certain time step. Blade structures are visible in the axial component, as well as the in-plane blade tip vortex system. Application of this approach to all 2700 snapshots generates a reconstructed, simplified, power filtered, transient flow field. Figure 12 explains the transient behavior of the flow, showing reconstructed fields for different timesteps compared to Figure 11. It is clearly visible, how the pattern moves through the side channel driven by the impeller below.

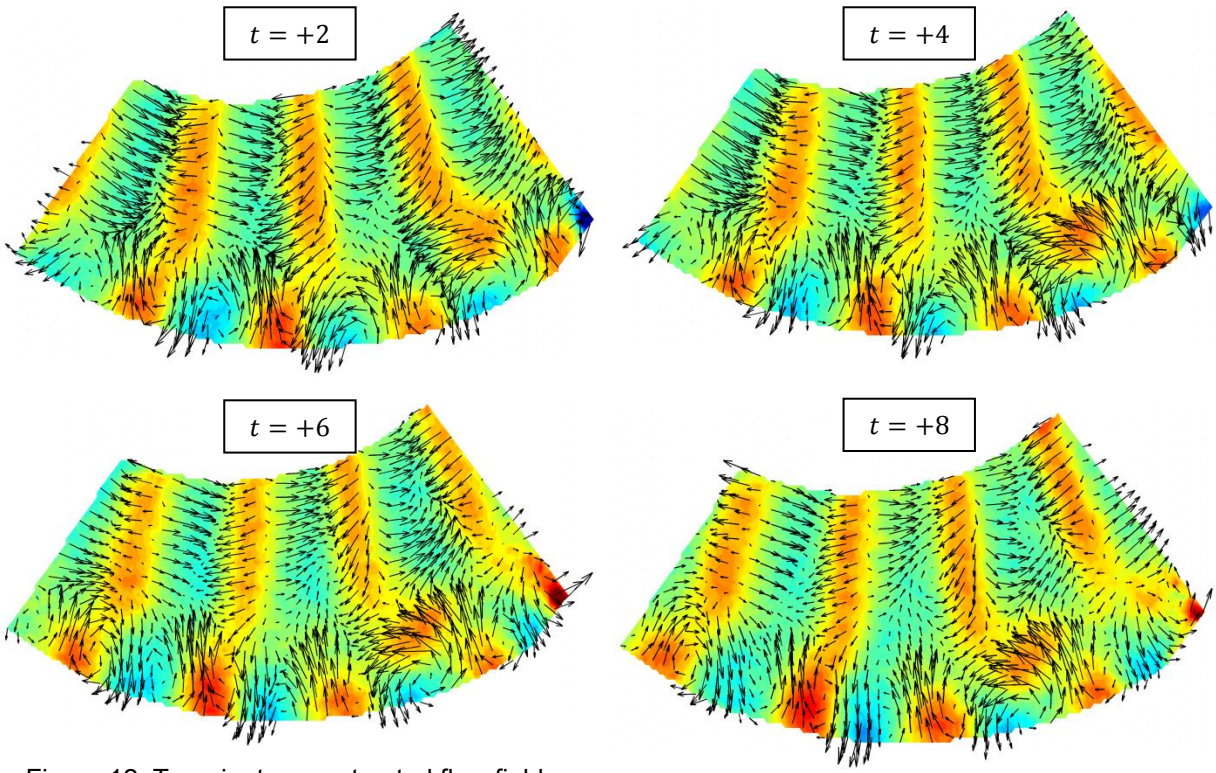

Figure 12: Transient reconstructed flow fields

Conclusion

The understanding of the highly complex and turbulent flow structure within a regenerative pump is crucial for further formulating the energy exchange between the impeller and the fluid. Even High Speed Stereo PIV Measurements analyzed in a classic approach give only limited information on the complex three dimensional swirl flow within the machine. The interacting flow patterns, which are the driving force behind the momentum exchange and therefore the working principle of the machine, are concealed by the highly energetic main flow. A simple subtraction of the average flow field from the instantaneous flow field gives a first impression of the vortex structures in game. However, without filtering the results are noisy and can even be misleading in case of sudden random disturbances in the flow field.
By using POD it is now possible to switch the point of view from the fixed laboratory system to the rotating blade related system without losing information. In a second step, by combining time resolved data, it is possible to apply an energy based filtering by only using strong modal components to reconstruct an instantaneous flow field. Once the all-concealing average flow field is subtracted, the POD method massively simplifies describing the flow within the machine. Particularly, the entire flow scenario can be approximated in good accuracy with only a few modes of salient flow patterns.
Therefore, it is now possible to focus on those structures and, in an upcoming approach, to identify the parameters of the machine generating those specific flow structures.
A deeper investigation of those phenomena will be the cause of upcoming projects.

Literature

[1] Mattern, P., Gabi, M., et al., 2014, „Investigations in a side channel pump using high speed stereo PIV", ISROMAC 15
[2] Holmes P, Lumley J L and Berkooz G 1996 Turbulence, Coherent Structures, Dynamical Systems, and Symmetry (Cambridge: Cambridge University Press)
[3] Aubry N 1991 On the hidden beauty of the proper orthogonal decomposition Theor. Comput. Fluid Dyn. 2 339–52
[4] Surek, D., 1997: "Turbulente Wirbelströmung und dynamische Druckschwankungen in Seitenkanalmaschinen", Forsch. Ingenieurwesen 63, pp. 85-101